International Journal of Heat and Mass Transfer 51 (2008) 5895–5905

Contents lists available at ScienceDirect

International Journal of Heat and Mass Transfer

journal homepage: www.elsevier.com/locate/ijhmt

Experimental study of onset of laminar–turbulent transition in mixed convection in a vertical heated tube

A. Behzadmehr [a,b], A. Laneville [a,*], N. Galanis [a]

[a] Génie mécanique, Université de Sherbrooke, Sherbrooke, QC, Canada J1K 2R1
[b] Mechanical Engineering Department, University of Sistan and Baluchestan, Zahedan, Iran

ARTICLE INFO

Article history:
Received 1 January 2008
Available online 13 June 2008

Keywords:
Mixed convection
Transition
Vertical tube
Thermal buoyant instability
Temperature fluctuations

ABSTRACT

Unsteady phenomena were observed in the case of airflows approaching transition inside a uniformly heated vertical tube. An analysis of the experimental data at three Reynolds numbers (Re = 1000, 1300 and 1600) allowed to establish that: (i) A flow instability onsets at different Grashof numbers (Gr) when the condition $Gr/Re > 1500$ is achieved. (ii) The FFT of the temperature signal shows a peak at a frequency f_D (0.45 Hz) when $Gr/Re > 1500$. (iii) This instability is associated to a thermal buoyant instability rather than to a thermal shear instability. (iv) This instability forms in the buffer region and then propagates towards the whole section of the tube as the Grashof number is increased.

1. Introduction

Experimental evidence compiled by Metais and Eckert [1] indicates that airflows inside a vertical tube with uniform heat flux can undergo transition from laminar to turbulent regimes for Reynolds numbers (Re) as low as 1000. For a given Reynolds number, the route to turbulence is one in which a radial temperature gradient destabilizes the otherwise laminar flow by accelerating the fluid close to the tube wall and causing a point of inflexion in the velocity profile (Lord Rayleigh's 1st Theorem). Scheel and Hanratty [2] studied experimentally the stability of flow in a vertical tube under mixed convection heat transfer by detecting temperature fluctuations in the effluent. They showed that the stability depends primarily on the shape of the velocity profile and only secondarily on the value of the Reynolds number. They found that the flow, when buoyancy assisted, first becomes unstable as the velocity profiles develop points of inflexion. They also mentioned that the temperature fluctuations, for low values of Re, are low frequency small scale oscillations. At larger values of Re, the initially regular fluctuations distort and grow in amplitude until fluctuations characteristic of turbulence such as a large scale periodicity appear. Yao [3] suggested that a buoyancy assisted flow is highly unstable and that its instability is supercritical. Except for a narrow range of Reynolds numbers, the disturbed flow has a double-spiral structure. Moreover, he showed that some of the unstable flows observed by Scheel and Hanratty [2] occurred in the developing region instead of in the fully developed region.

The importance of the Prandtl number in mixed convection stability was studied by Yao and Rogers [4]. They showed that thermal shear perturbations occurring in low Prandtl number fluids as the Rayleigh number is increased, initiate a linear instability that distorts the velocity profiles sufficiently to destabilize the flow. In larger Prandtl number fluids, however, the flow becomes unstable to the thermal buoyant perturbations induced locally by the temperature fluctuations: this local disruption of the buoyant force in turn causes a distortion of the velocity field by a transfer of kinetic energy from the fluctuating buoyant potential. Chen and Chung [5] investigated the linear stability of mixed convection flow in a vertical channel. The flow, when buoyancy assisted, is dominated by two dimensional disturbances and its stability is strongly dependent on the Prandtl number. They showed that the instability characteristics for some case of channel flow are significantly different from the results for heated annulus and pipe flows. Su and Chung [6] analyzed the linear stability of mixed convection in a vertical tube. They showed that the flow can become unstable at low Reynolds number and Rayleigh number irrespective of the Prandtl number. Their results show that the Prandtl number plays an active role in buoyancy assisted flow and is an indication of the viability of kinematic or thermal disturbances. They also showed that for assisted flow with $Pr < 0.3$ the thermal shear instability is dominant while for $Pr > 0.3$, the assisted–thermal buoyant instability becomes responsible. If the Grashof number (or the heat flow at the wall) is sufficiently increased, the velocity gradient produces a shear from which originates a periodic or wavy structure. The visualization of the flow field in a vertical tube subjected to a uniform wall heat flux carried out by Bernier and Baliga [7] points to this route leading to the laminar–turbulent transition. Behzadmehr

* Corresponding author. Fax: +1 819 821 7163.
E-mail address: andre.laneville@USherbrooke.ca (A. Laneville).

0017-9310/$ - see front matter © 2008 Elsevier Ltd. All rights reserved.
doi:10.1016/j.ijheatmasstransfer.2008.04.005

Nomenclature

A	tube cross sectional area
C_p	specific heat
D	internal tube diameter
ES	thermal shear production, $-\langle U_{sd}U_{sd}\frac{dU}{dr}\rangle$
EB	thermal buoyant turbulent production, $\frac{Gr}{4Re^2}\langle U_{sd}T_{sd}\rangle$
f	frequency
g	acceleration of gravity
Gr	Grashof number, $g\beta D^4 q_w/\lambda\nu^2$
L	length of test section
$\dot{m}$	mass flow rate
Nu	Nusselt number
P	pressure
Pr	Prandtl number
q_w	uniform heat flux at the solid–fluid interface
r	radial coordinates
Re	Reynolds number, U_bD/ν
Ri	Richardson number, Gr/Re^2
T, T'	time averaged and fluctuating temperature
U, U'	time averaged and fluctuating velocity indicator
Z	axial coordinates

Greek letters

β	volumetric expansion coefficient
λ	thermal conductivity
μ	dynamic viscosity
ν	kinematic viscosity
ρ	density

Subscripts

0	inlet condition
b	bulk
c	centreline
L	tube outlet
sd	standard deviation
w	wall

et al. [8,9] implemented a numerical procedure that models laminar as well as turbulent flow to study mixed convection of air flowing through a vertical tube with uniform wall heat flux. The results of their numerical simulations indicate two laminar–turbulent transitions at Reynolds number as low as 1000. The effects of inlet turbulent intensity on the axial evolution of the hydrodynamic and thermal fields as well as on the developed velocity and temperature profiles are presented by Behzadmehr et al. [10]. They found that the flow regime is influenced by the inlet turbulence intensity and by the Grashof number. For a given Pr and Re, increasing inlet turbulent intensity (inlet disturbances) decreases the Gr for which flow regime changes from laminar to turbulent. However, for higher value of the inlet turbulent intensity, the same Re and Pr, higher value of the Gr is needed for which flow regime change back to laminar (re-laminarization).

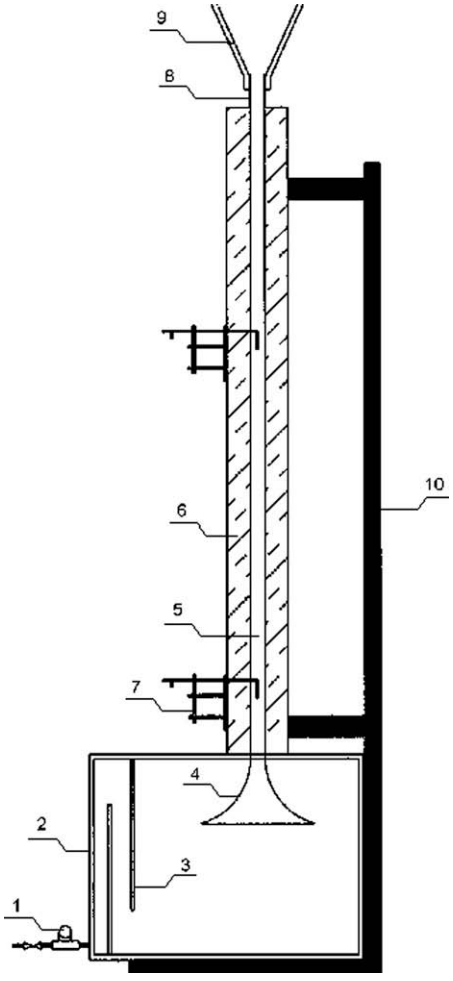

Fig. 1. Sketch of experimental apparatus.

Table 1
Estimated uncertainties

Item	Uncertainties
Mass flow meter	±2% of reading value
Temperature	±0.05 °C
Thermocouple location	±1.2 mm
Pitot tube location	±2.2 mm
Radial position of Pitot tube	±0.03 mm
Pressure transducer	±0.024 Pa
Manometer	±0.024 Pa

In the case of airflows undergoing transition, the temperature and velocity fluctuations have not been studied in detail neither experimentally nor numerically. An experimental apparatus was therefore designed in order to examine the characteristics of these fluctuations as transition onsets in the case of low Reynolds numbers. Since the Prandtl number for air is of the order of unity, a correlation should exist between the temperature fluctuations and the velocity fluctuations: the signal of the fluctuating temperature should give some insight on the flow transition [11]. This article deals with an analysis of the nature of the temperature and velocity fluctuations using experimental data obtained at $Re = 1000$, 1300 and 1600 over a wide range of the Grashof numbers. A signal analysis is presented to show the details that could characterize onset of laminar–turbulent transition.

2. Experimental set-up and procedure

2.1. Experimental apparatus

Fig. 1 shows a schematic view of the experimental set-up. It consists of two principal components: a settling chamber used to

condition the air and a long heated tube. The ensemble is connected to the laboratory air network via a filter and a pressure regulator. Air flows through a digital mass flow meter (No. 1) and enters into the settling chamber (No. 2) and exits through the nozzle (No. 4) once its inlet jet shape has been broken by its passage through two baffles (No. 3). Downstream of the nozzle, a uniform airflow enters into the test section, a 50.87 mm internal diameter tube (No. 5) on the external wall of which are mounted twelve thermocouples to measure the temperature; two holes are machined to traverse the Pitot tubes and thermocouples in the radial direction. Flexible heating tapes are uniformly wrapped around the test tube and the entire assembly is covered with a fibreglass pipe insulating material (No. 6). Two supports (No. 7), designed to traverse the Pitot tubes in the radial direction, are aligned with the machined holes at $Z/D = 6.81$ and $Z/D = 45$. The choice of these two positions will be discussed later in 3.1. The downstream end of the test tube is fitted with a small piece of PVC tube (No. 8) to reduce the wall conduction; a diffuser (No. 9) terminates the test tube assembly and discharges the airflow into the environment. All the foregoing elements are installed on a chassis (No. 10). Uncertainties of the components are presented in Table 1.

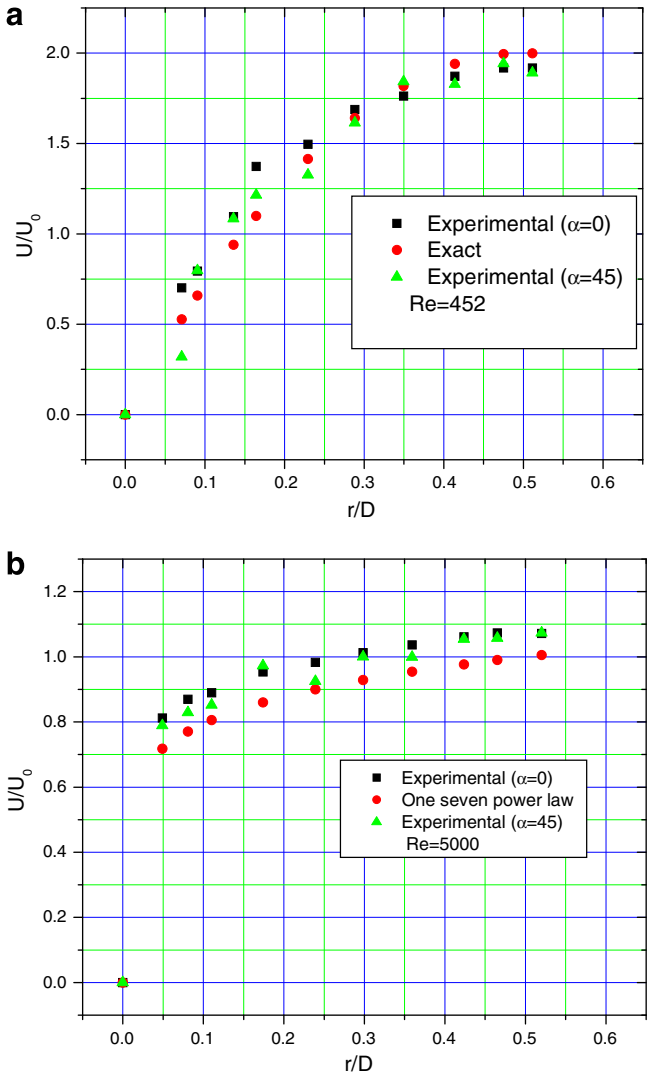

Fig. 2. Comparison of the mean axial velocity with the analytical solution. (a) Laminar flow and (b) turbulent flow.

2.2. Temperature and dynamic pressures measurements

Wall temperatures were measured using type *K* thermocouples mounted at different axial positions ($Z/D = 1.45, 6.38, 11.30, 16.22, 21.14, 26.06, 30.98, 40.83, 50.67, 60.52, 65.43, 70.16$). Two additional thermocouples (type *K*) were mounted on the Pitot tubes to measure the radial distribution of the air temperature (axial positions: $Z/D = 6.81$ and $Z/D = 45$). Air temperatures, in the environment, in the settling chamber and at the exit diffuser, were also measured using type *K* thermocouples.

The radial distribution of the mean velocity and its fluctuations at $Z/D = 6.81$ and $Z/D = 45$ were measured using Pitot tubes. Two types of corrections were applied to the measured mean dynamic pressures: the first, required in the case of low velocities and the second, required in the case of wall proximity as the tube is traversed to measure the velocity profile. In the case of low flow velocities, the Reynolds number based on the Pitot tube characteristic length is less than 50 and the viscous effects due to the boundary layer developing on the tube surface differ from those in standard testing conditions; the static pressure tap is consequently misplaced to measure the equivalent upstream static pressure of the flow; the correction technique suggested by AirFlow Development [12] was applied. The effect of wall proximity was corrected using the method suggested by Paradis [13]. In turbulent flow regimes, the corrections applied to the measured values of the velocity amount to 10% and 13%, respectively, at $r/D = 0$ and $r/D \cong 0.5$; in laminar flow regimes, they corresponded to 15% and 18%, respectively. The line connecting the Pitot tube to the pressure transducers is rigid vinyl tubing with an internal diameter chosen to preserve the frequency content of the pressure fluctuations from attenuation at frequencies less than 25 Hz. The value of the mass flow rate was continuously monitored using a digital mass flow meter; the measured value was recorded simultaneously with that of the pressure transducers and thermocouples. The uniform heat flux for calculating the Grashof number was determined by measuring the bulk temperature at $Z/D = 6.81$ and $Z/D = 45$ and with using an energy balance equation ($q_w \pi DL = \rho U_0 A C_p\ (T_{b2} - T_{b1})$). The calculated value of the heat flux was confirmed by measuring the input voltage and current to the heating tapes: the net uniform heat flux transferred to the fluid was then calculated using an energy balance taking into account the heat losses. More details are given in Section 3.1 (Validation). A period of 2.5 h was required for the set-up to reach the steady state conditions.

2.3. Data acquisition system

The acquisition system consists of an AT-MIO-16XE-50 board installed in a personal computer and an AMUX-64T multiplexer unit. Low pass filters set at a cut-off frequency of 10 Hz were introduced at the level of the multiplexer in order to remove the environmental noises from the thermocouples and pressure transducers signal. The data acquisition was performed using a program developed under the commercial software Labview. The sampling rate of the data acquisition system was set at 5 samples per second for each channel and data were recorded over a period of more than 90 s for each test.

3. Results and discussion

3.1. Validation of the set-up and of the procedure

In addition to the calibration of each sensor, several tests were performed to validate the set-up: they include the measurement of the velocity profiles in laminar and turbulent unheated flows as well as the longitudinal distribution of the bulk temperature in

heated flows. Once the set-up was validated, a procedural routine was developed and applied to each set of measured data to insure its validity. The details of the validations follow.

The ability of the set-up to produce a given flow was verified by the measurement of the velocity profile under laminar and turbulent conditions in the case of unheated pipe; its ability to produce uniform heat flux conditions was also verified by comparing the measured longitudinal profile of the bulk temperature to the analytical results of an energy balance in the case of the uniformly heated pipe. Fig. 2a and b compare the measured velocity profiles at $Z/D = 45$ in the cases of unheated flow regimes at $Re = 452$ and $Re = 5000$ to the analytical solution for laminar fully developed flows and to the power law equation for turbulent flows in a circular tube. In the case of laminar flows, the discrepancy between the results on the centreline is less than 4% while near the wall it amounts to about 15%. The corresponding discrepancy for the turbulent flow conditions is 6% and 9%, respectively. The accuracy of the one-seventh law is reason for the higher discrepancy in the case of turbulent flow at the centreline region compared to the laminar flow. The circumferential symmetry of the velocity profiles was verified at 45°. Fig. 3 shows that the measured bulk temperature, with the heating system turned on, increases in the flow direction with a slope of 0.0058, a value close to the analytical one, $4/(Re \times Pr)$, derived from the energy balance in the case of the flow in a tube with uniform heat flux profile. Fig. 3 includes the measured wall temperatures along the tube.

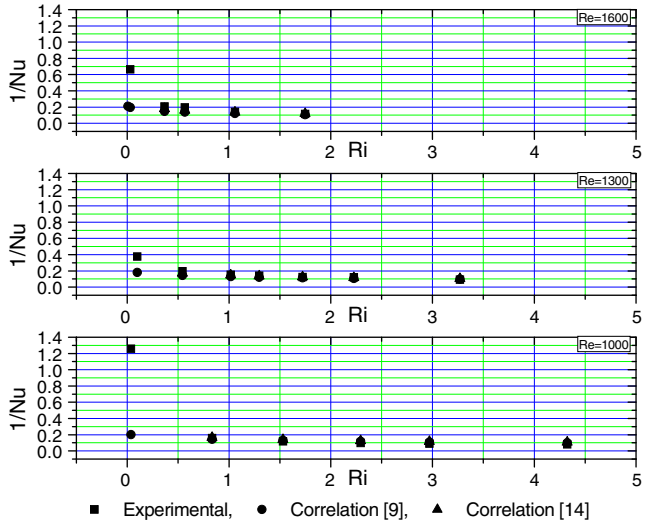

Fig. 5. Comparison of the measured $1/Nu$ with different correlations.

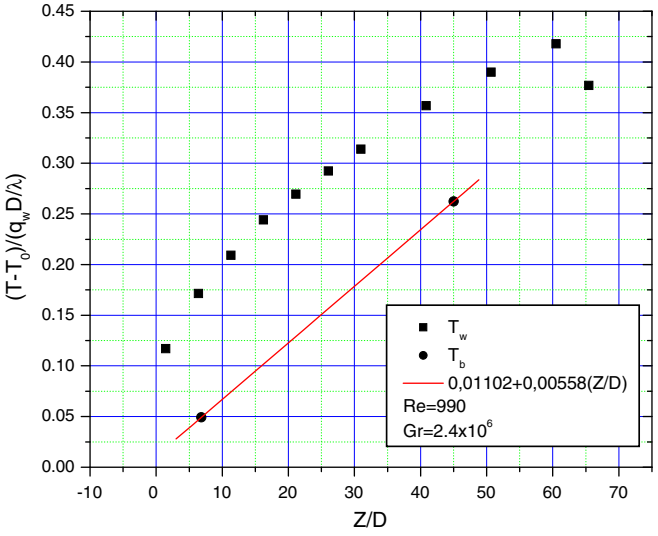

Fig. 3. Non-dimensional wall and bulk temperature.

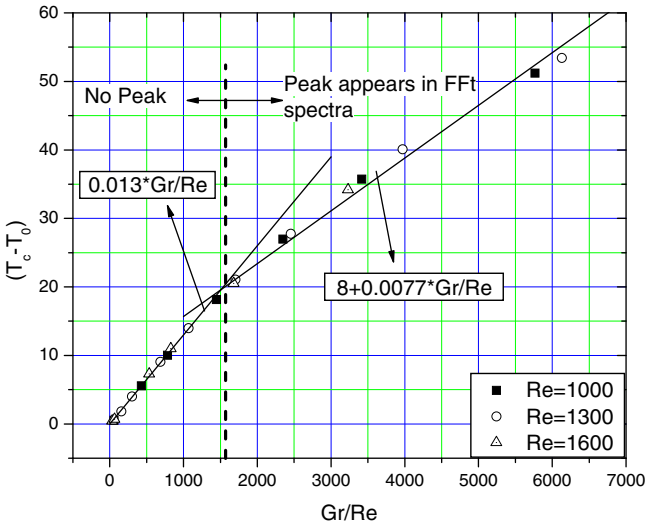

Fig. 6. Variations of $(T_c - T_0)$ for different Re–Gr combinations at $Z/D = 45$.

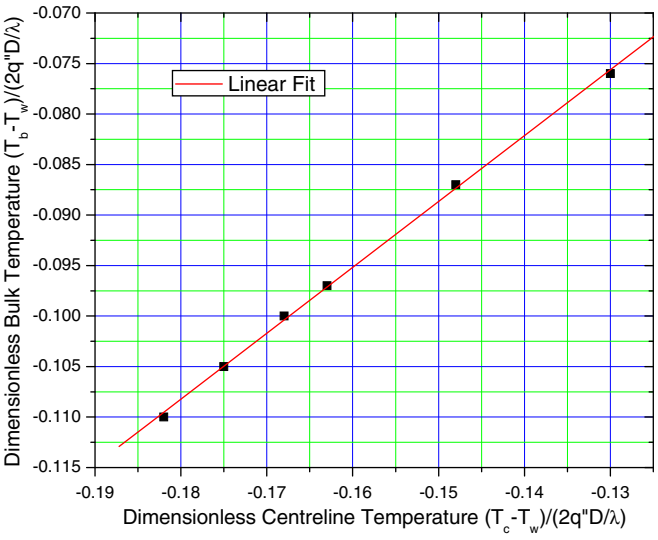

Fig. 4. Dimensionless bulk and centreline temperatures based on Hallman [14] analytical solution.

The steady state heat losses in this experimental set-up were determined in a procedure taking into account an energy balance over the entire set-up: the electrical power fed to the heating tape is assumed to be converted in three components, the radial heating power in the direction of the air flow, the radial heat losses through the insulating material covering the heating tape and that at both ends of the tube. The conduction heat losses at the upstream end of the tube act as a preheating of the airflow inside the converging nozzle. This preheating effect due to the axial wall conduction is observed in Fig. 3 by a non-dimensional bulk temperature larger than zero at the tube inlet (since T_b should be T_0 theoretically). The axial heat loss in the wall at the downstream end of the test section is also observed (Fig. 3) to propagate significantly in the range $Z/D > 60$ and less in the range $50 < Z/D < 60$. The location $Z/D = 45$ was then selected in order to explore its flow properties; an upstream position as close as possible to the inlet, $Z/D = 6.81$, was also selected in order to establish the flow inlet conditions

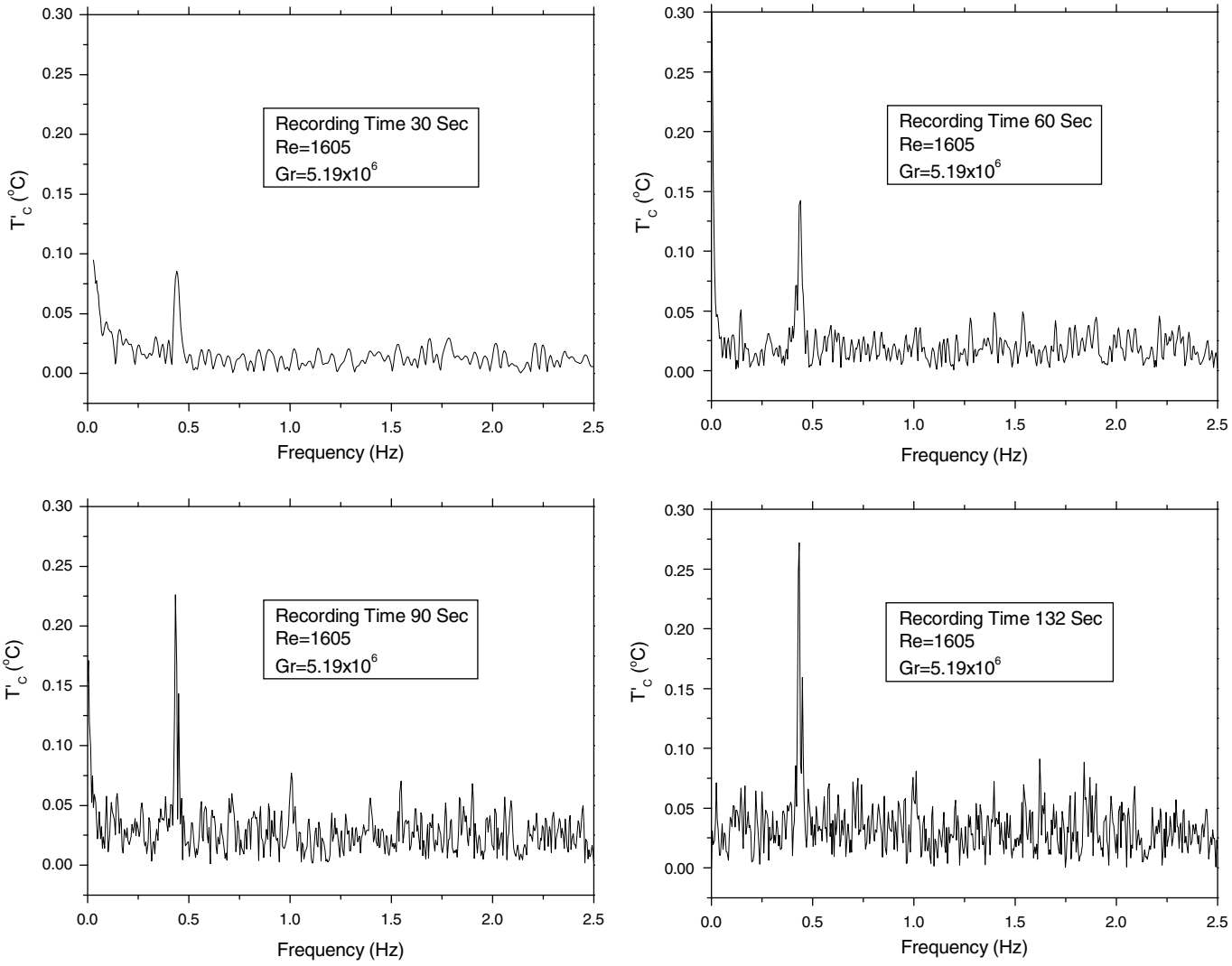

Fig. 7. Effect of recording time on the FFT spectrum of the temperature.

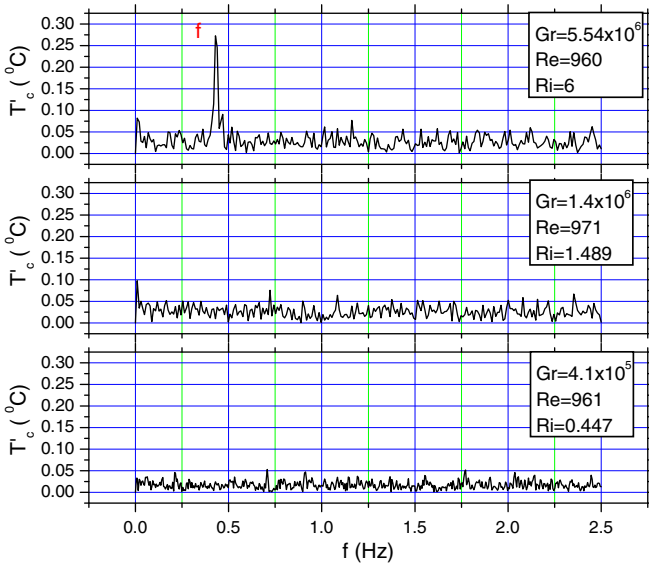

Fig. 8. FFT spectrum of the temperature fluctuations for $Re \approx 1000$ at $Z/D = 45$.

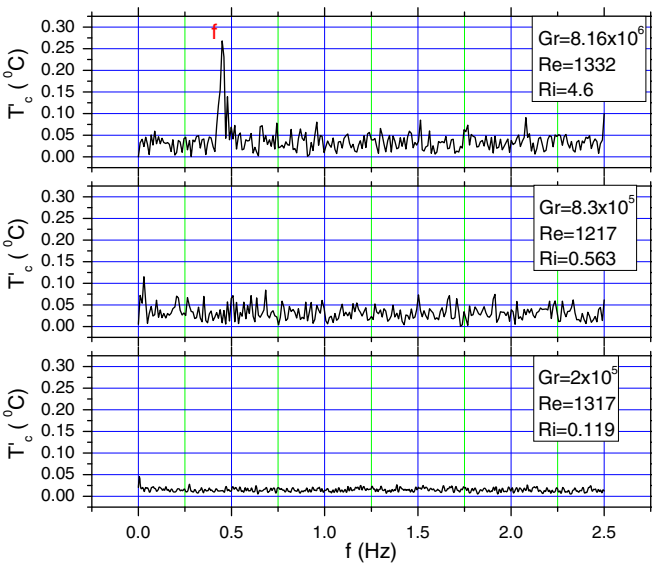

Fig. 9. FFT spectrum of the temperature fluctuations for $Re \approx 1300$ at $Z/D = 45$.

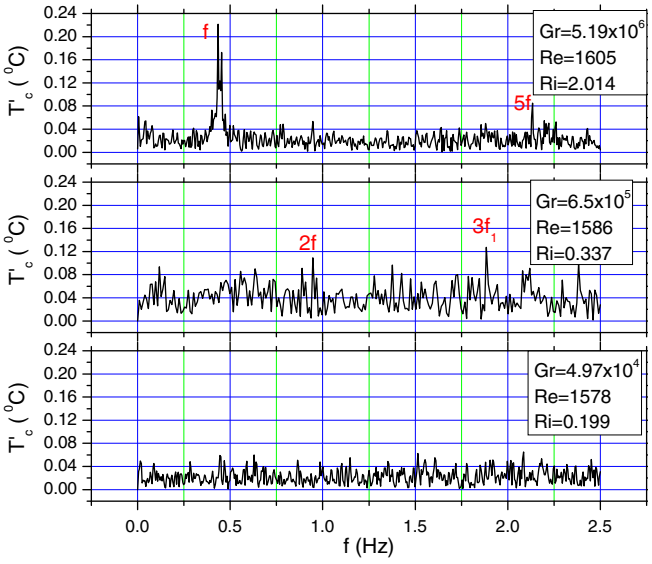

Fig. 10. FFT spectrum of the temperature fluctuations for $Re \approx 1600$ at $Z/D = 45$.

Table 2
Reynolds and Grashof numbers and their corresponding incertitude in the case of the tests reported in Figs. 8–10

Re	*Gr*	*Ri*
961 ± 16%	$4.10 \times 10^5 \pm 14\%$	0.441
971 ± 18%	$1.40 \times 10^6 \pm 16\%$	1.489
960 ± 18%	$5.54 \times 10^6 \pm 15\%$	6.002
1317 ± 9%	$2 \times 10^5 \pm 9\%$	0.119
1217 ± 10%	$8.3 \times 10^5 \pm 9\%$	0.563
1332 ± 9%	$8.16 \times 10^6 \pm 8\%$	4.600
1578 ± 6%	$4.97 \times 10^4 \pm 14\%$	0.199
1586 ± 7%	$8.5 \times 10^5 \pm 6\%$	0.337
1605 ± 7%	$5.19 \times 10^6 \pm 6\%$	2.014

as well as to determine the effective wall heat flux over the range $6.81 \leqslant Z/D \leqslant 45$ with redundancy.

The relation between the dimensionless centreline and bulk temperatures (as defined in the analytical solution proposed by Hallman [14] for fully developed laminar mixed convection with uniform heat flux in a vertical tube) is shown in Fig. 4. The existence of the relation between these two temperatures for the laminar mixed con-

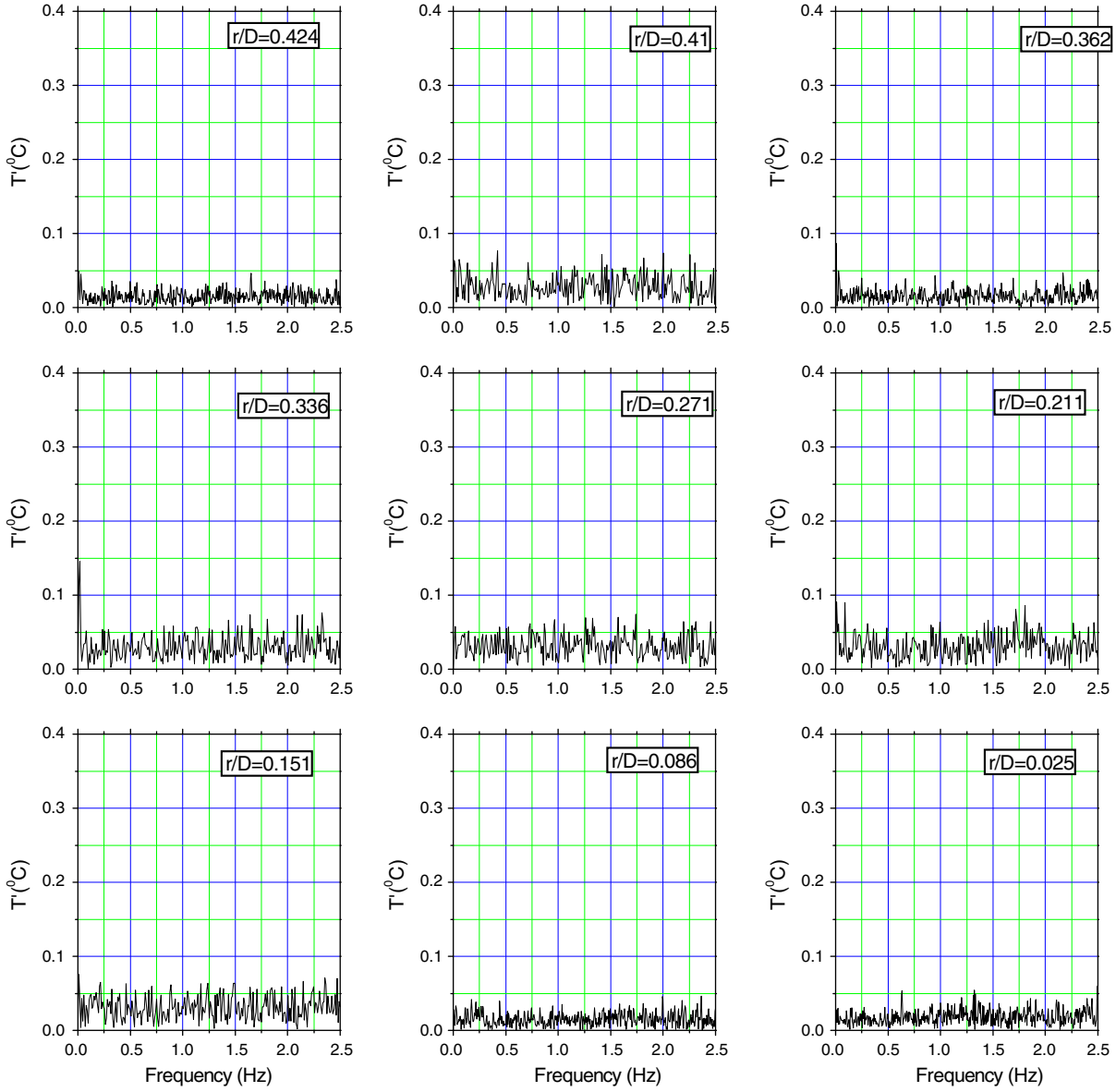

Fig. 11. FFT spectrum of the temperature fluctuations for $Re = 958$ and $Gr = 1.09 \times 10^6$ at different radial positions ($Z/D = 45$).

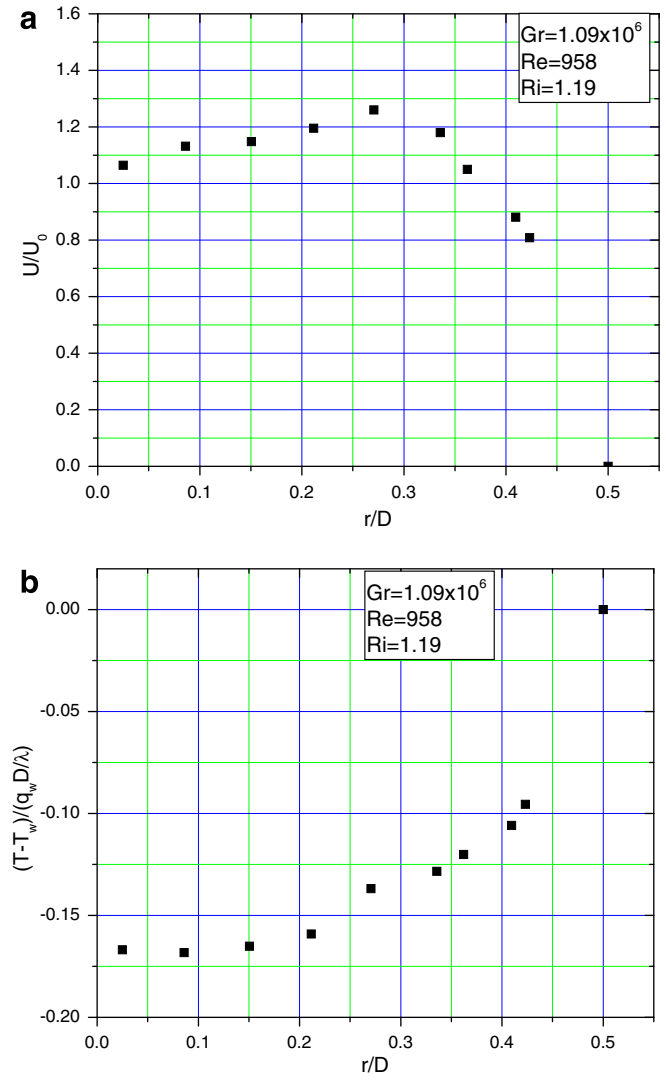

Fig. 12. Variations of (a) dimensionless axial velocity and (b) dimensionless mean temperature, at different radial positions ($Z/D = 45$) for $Re = 958$ and $Gr = 1.09 \times 10^6$.

vection flow allows us to investigate the mean flow using the measured temperature at $r = 0$ as representative of the bulk temperature.

To ascertain the ability of the setup for reproducing the other experimental or theoretical results, the measured values of $1/Nu$ versus Ri are compared with the corresponding theoretical and other experimental results. Fig. 5 compares the inverse of the measured Nusselt ($1/Nu$) with the correlations proposed by Behzadmehr et al. [9] and Hallman [14] for laminar mixed convection. The agreement is good except for the lower Ri (closed to zero). Difference between the wall, bulk and inlet temperatures at low Gr is very small; the incertitude of temperature measurement becomes more important.

3.2. Analysis of the data

3.2.1. Thermal parameters: mean values

In the case of the flow inside a uniformly heated tube, the bulk temperature is well known to vary linearly along the tube. Already the energy balance over the entire test section has been used in Section 2.2 and can be re-written in order to introduce the Grashof and Reynolds numbers and to define this "constant of linearity" (units of inverse temperature) as follows:

$$\pi D L q_w = \dot{m} C_p (T_b - T_0) \Rightarrow q_w = \frac{D \rho U_0 C_p}{4L} (T_b - T_0) \quad (1)$$

Substitution of q_w in the Grashof definition gives:

$$Gr = \frac{\rho g \beta D^4 C_p}{4 \lambda L \nu} \frac{U_0 D}{\nu} (T_b - T_0) \Rightarrow \frac{Gr}{Re} = C(T_b - T_0) \quad (2)$$

where $C = \frac{\rho g \beta D^4 C_p}{4 \lambda L \nu}$ can now be considered a "constant". In this case, since the Reynolds and Grashof numbers have been evaluated at the entry conditions, the value of C has been determined using the properties at the tube inlet. As shown in Fig. 4, the centreline temperature qualitatively represents the bulk temperature; the constant C may be then evaluated qualitatively and compared to the slope of the reduced data. Fig. 6 shows the variation of $(T_c - T_0)$ at $Z/D = 45$ as a function of Gr/Re in the case of three different Reynolds numbers. As expected, the temperature difference increases with the Gr/Re; however the slope of temperature difference changes for $Gr/Re > 1500$. The slope of the data in the first portion is measured at 0.013 ($1/C = 0.013$ at $T_0 = 21$ °C, a temperature mostly present during the tests). The slope of the data in the range $Gr/Re > 1500$ changes by a factor of 1.7, to the value of 0.0077 (to get $1/C = 0.0077$, the temperature required at the inlet should be less than 0 °C). Since the uncertainty associated with the temperature measurement, Gr and Re is very small, it is therefore reasonable to consider this variation of slope or "point of deviation" as an indicator of a possible modification of the flow regime worth exploring.

3.2.2. Thermal parameters: unsteady values

The mean values of the thermal parameters have been studied extensively in the literature while the unsteady behavior has not been studied in detail; these unsteady data are presented over a wide range of Re–Gr combinations in this section. Using the signal of the fast response thermocouple, the frequency spectrum of temperature fluctuations (T_c') were then measured and analyzed. The recording time (more than 90 s) was sufficiently long to capture the repeatability of the fluctuations and any possible bursts. Fig. 7 shows the effect of the recording time on the FFT results. The figure shows clearly that the recording time (about 90 s) is long enough for studying the unsteadiness of the temperature signal. It should be emphasized that this study is not intended to assert the amplitude of any instability or fluctuation but rather the frequency of their occurrence.

Figs. 8–10 show the frequency spectrum of temperature fluctuations, respectively, for $Re \approx 1000$, 1300 and 1600; each figure includes the spectrum obtained for three different heat flux levels chosen in order to detect changes in the temperature fluctuations. Table 2 gives the Re, Gr and the Richardson numbers and their corresponding incertitude for the nine spectra of Figs. 8–10.

The striking event in these figures is the amplification of a periodic phenomenon at the frequency, $f = 0.45$ Hz, for the three conditions (Re, Gr, Gr/Re^2) = (960, 5.54×10^6, 6), (1332, 8.16×10^6, 4.6) and (1605, 5.19×10^6, 2.014); referring to Fig. 6, this amplification occurs in the range $Gr/Re > 1500$ and is absent for $Gr/Re < 1500$. The temperature spectrum for low Gr shows a flat distribution but with mean and standard deviation values increasing with the Grashof number. These observations point to a combination of two phenomena as the Grashof number is increased under laminar conditions: the onset of a periodic flow structure at a fixed frequency (that differs from the Helmoltz frequency) and an increase of the levels of the random fluctuations.

In order to scrutinize this phenomenon, temperature fluctuations are examined at different radial positions for three different Re–Gr combinations: the first combination prior to the occurrence of the peak, the second one, very close to its first occurrence, and the third combination at a much higher value than the Re–Gr of the first occurrence.

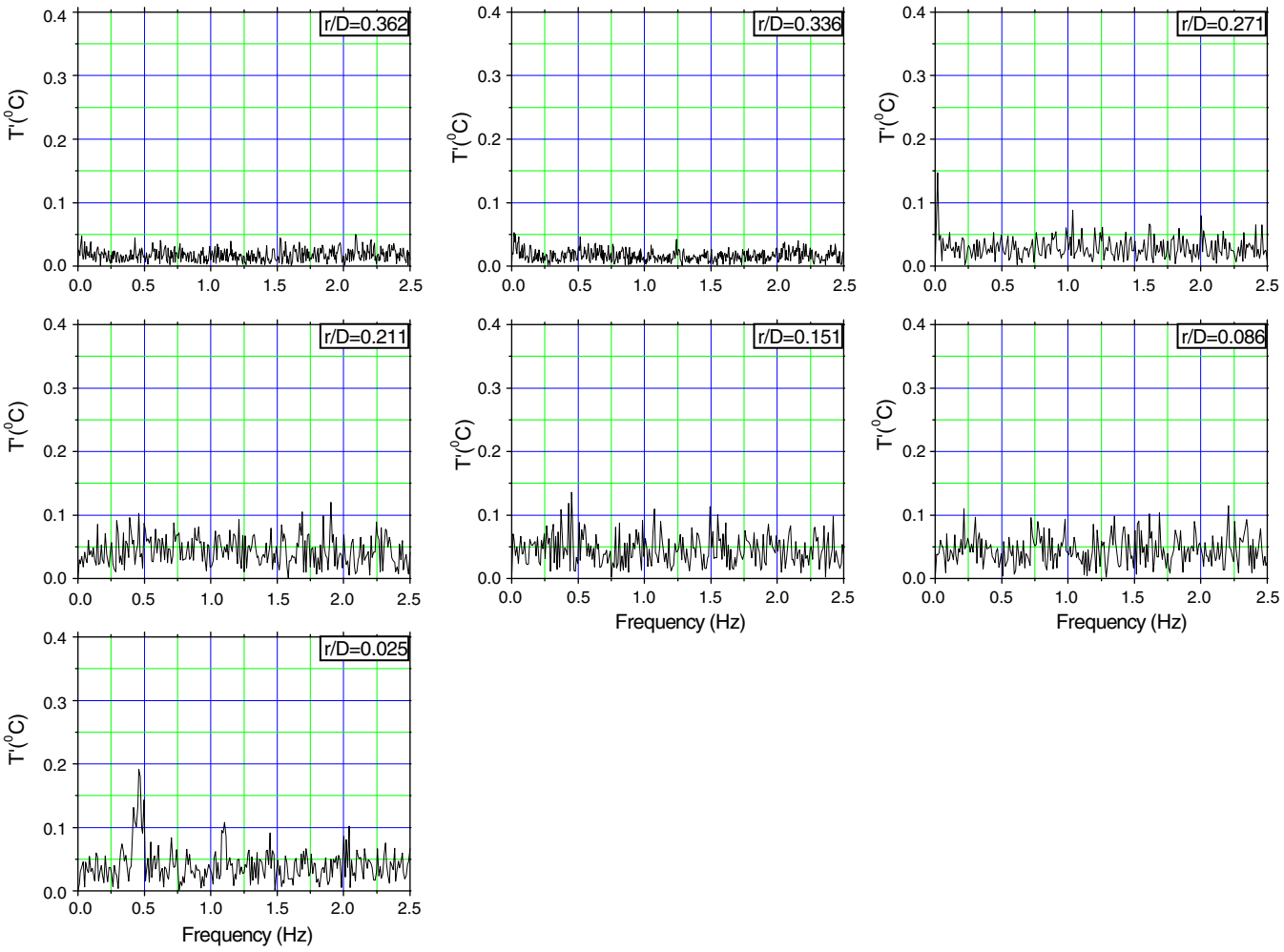

Fig. 13. FFT spectrum of the temperature fluctuations for $Re = 961$ and $Gr = 1.8 \times 10^6$ at different radial positions ($Z/D = 45$).

Fig. 11 shows the results of a FFT analysis of the temperature fluctuations for $Re = 958$ and $Gr = 1.09 \times 10^6$ ($Gr/Re = 1137$). In this case, the frequency distribution of the temperature fluctuations at each radial location does not vary much; it is a flat distribution with intensity of the order of the noise level. Nevertheless, in the region $0.15 < r/D < 0.35$, the temperature fluctuations are more important than the ones near the wall and the centreline region ($0 \leqslant r/D < 0.35$).

In order to determine the relative importance of the temperature fluctuations, their local mean velocity and temperature profiles are, respectively, shown in Fig. 12a and b. As expected under laminar and low heating conditions, heat propagates essentially near the tube wall, the core of the flow remaining at almost a uniform mean temperature. But in the region $0.15 < r/D < 0.35$, a maximum ($r/D_{\text{maximum}} \sim 0.27$) and a point of inflexion ($0.15 < r/D_{\text{inflexion}} < 0.2$) appears in the velocity profile as shown in Fig. 12a. These variations are higher than the corresponding uncertainty of the velocity measurements.

The corresponding profiles measured in the case of the same Reynolds number ($Re = 961$) but higher Grashof number (1.8×10^6, $Gr/Re = 1873$) are shown in Figs. 13 and 14. The results of the FFT analysis of the temperature fluctuations (Fig. 13) indicate that the level of the frequency distributions increases in all regions except near the wall region. A significant peak is observed in the distribution for the 0.45 Hz frequency only at the centreline ($r/D = 0{,}025$). Fig. 15 is highly instructive. The measured velocity profile (Fig. 14a) shows that the point of inflexion ($0.1 < r/D_{\text{inflexion}} < 0.15$) as well as the maximum ($r/D_{\text{maximum}} \sim 0.21$) are closer to the center of the tube. The heat from the wall has reached farther inside the tube, as expected and shown in Fig. 14b. The instability may now be inferred to originate from the buffer region ($0.15 < r/D < 0.35$) where the point of inflexion appears in the velocity profile, to propagate towards the centreline and to be amplified in the centreline region. It can be explained by the variation of the fluid viscosity at radial positions. Viscosity may destabilize the flow through the Reynolds stresses; however it could stabilize the flow through the effect of viscous dissipation [6]. Since the viscosity of the fluid at higher temperature near the wall is larger than that at the other regions, viscous dissipation near the wall region therefore stabilizes the fluid flow whereas the temperature fluctuations are amplified in the centreline region.

Fig. 15 presents the distributions of the temperature fluctuations at $Ri = 1.422$ ($Re = 1479$, $Gr = 3.11 \times 10^6$ or $Gr/Re = 2102$), a much higher Richardson number than the one for which the peak would occur at "the point of deviation" ($Ri = 0.723$ if $Gr = 3.11 \times 10^6$ and $Gr/Re = 1500$). It shows that the level of the fluctuations is high in all the regions (near wall, buffer and centreline regions). The peak in the distributions of the fluctuating temperature is present throughout the cross section and at the same 0.45 Hz frequency.

Using the additional Fig. 15, the comparison of the three sets indicates that the fluctuations are first generated in the buffer region

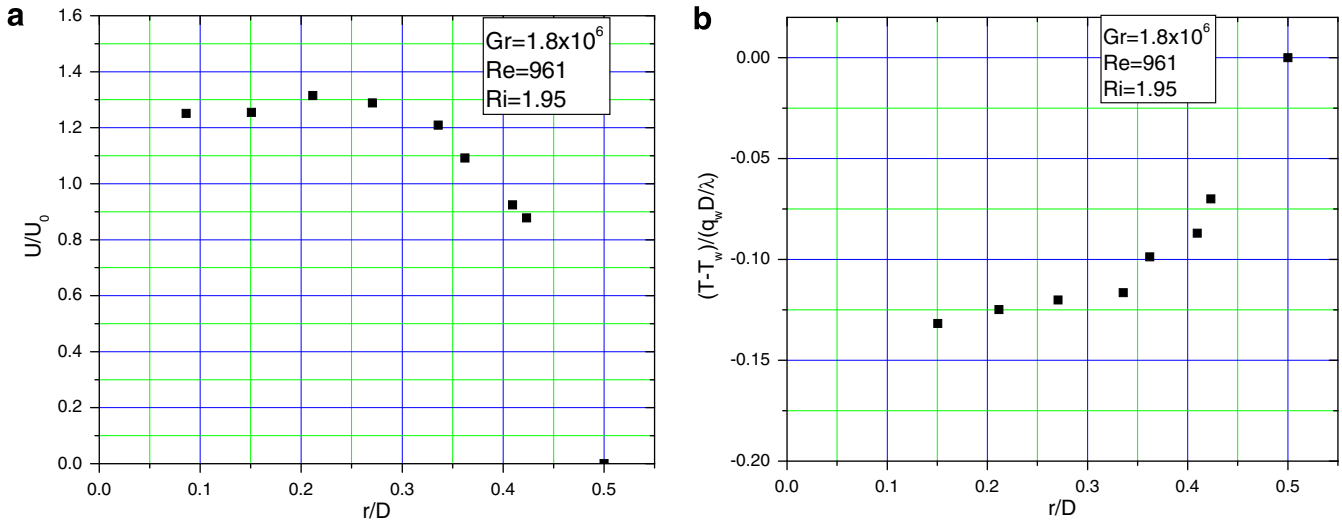

Fig. 14. Variations of (a) dimensionless axial velocity and (b) dimensionless mean temperature, at different radial positions ($Z/D = 45$) for $Re = 961$ and $Gr = 1.8 \times 10^6$.

(where a point of inflexion appears in the velocity profile) and then propagate to the centreline region to cause a wavy structure with a significant frequency (0.45 Hz); this wavy structure finally diffuses towards the wall region and covers the entire region with the same dominating frequency (≅0.45 Hz). The corresponding velocity and temperature profiles are also shown in Fig. 16a and b.

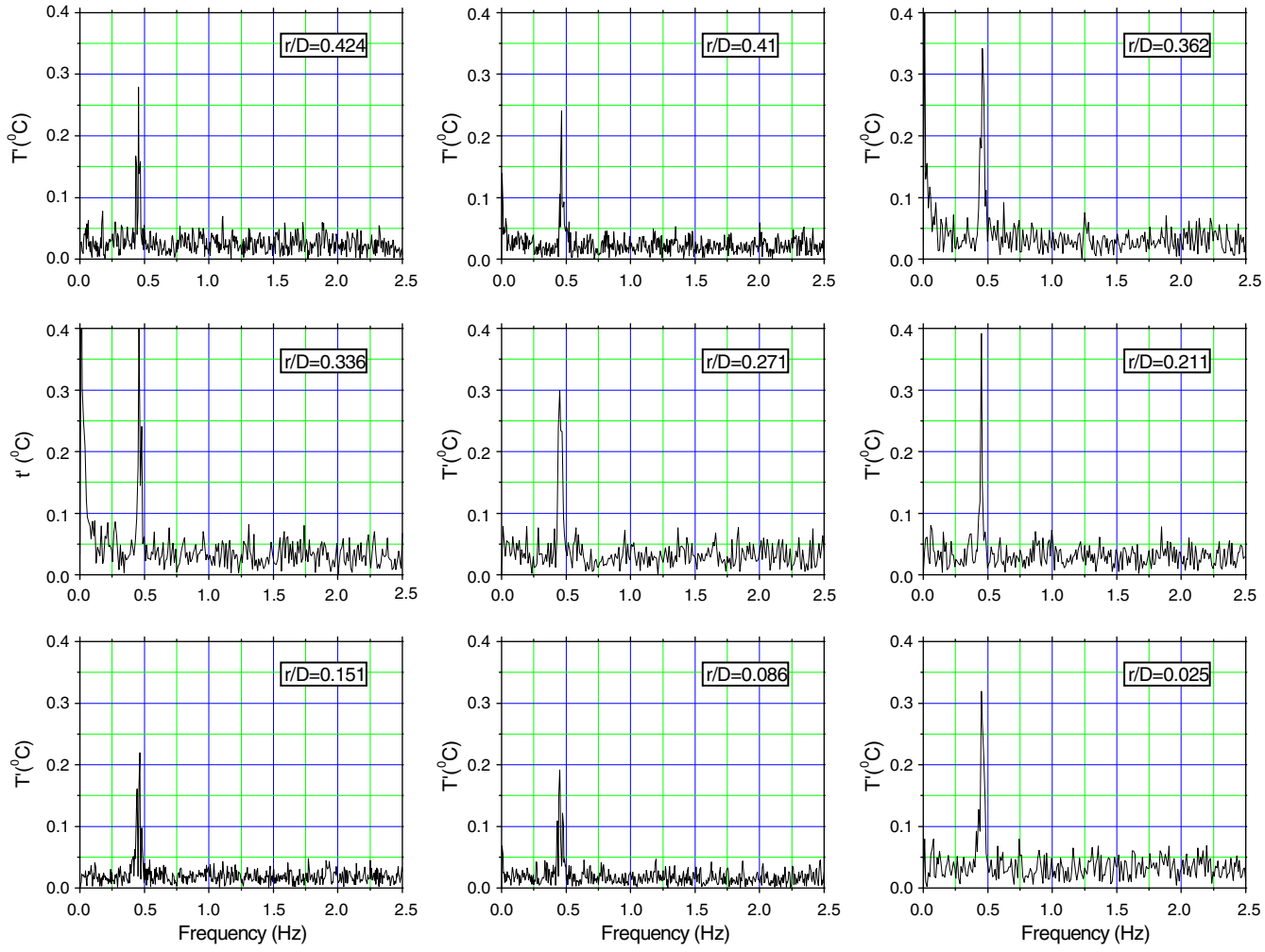

Fig. 15. FFT spectrum of the temperature fluctuations for $Re = 1479$ and $Gr = 3.11 \times 10^6$ at different radial positions ($Z/D = 45$).

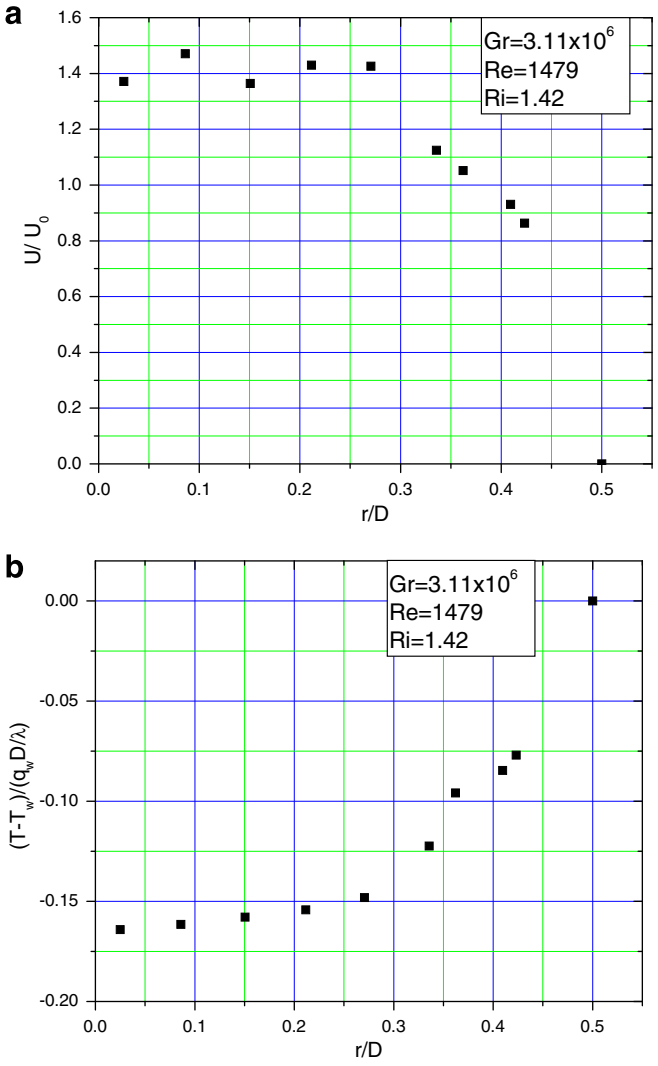

Fig. 16. Variations of (a) dimensionless axial velocity and (b) dimensionless mean temperature, at different radial positions ($Z/D = 45$) for $Re = 1479$ and $Gr = 3.11 \times 10^6$.

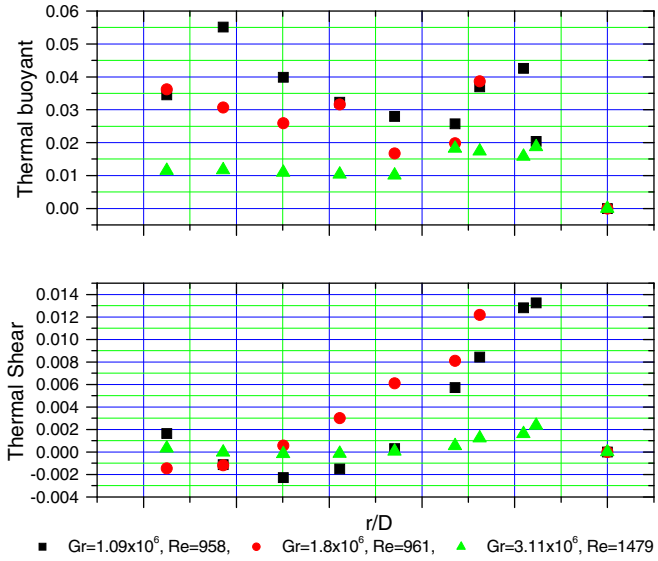

Fig. 17. Energy budget. (a) Thermal buoyant and (b) thermal shear.

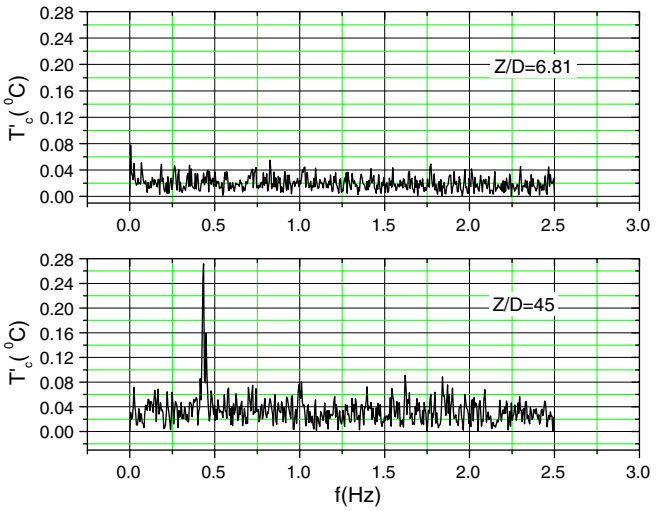

Fig. 18. FFT spectrum of the temperature fluctuations at two different axial positions.

3.2.3. Energy budget considerations

In order to better assess the origins of this thermal instability at 0.45 Hz, the terms of the kinetic energy budget [5] were evaluated and compared in the case of the three foregoing *Re–Gr* combinations. The kinetic energy budget contains two productions and one dissipation term. The first production term, ES, also present in isothermal flows, is the shear production term resulting from the product of the Reynolds stress and the mean flow strain rate. In the present set-up, the mean velocity strain rate can be calculated using the velocity profile but the unmeasured Reynolds stresses is conservatively replaced by the square of the standard deviation of streamwise fluctuating velocity.

The second production term, EB, absent in isothermal flows, represents the work done by the thermal buoyant potential of the temperature fluctuations. It includes the fluctuating variables U_{sd} and T_{sd}, both measured in the present set-up. The dissipation term represents the energy losses through molecular viscosity.

Then the driving process of the flow instability may be determined by comparing the production of the kinetic energy perturbations. Fig. 17 shows the profile of both the thermal buoyant production ($EB = \frac{Gr}{4Re^2}\langle U_{sd}T_{sd}\rangle$) and the thermal shear turbulent kinetic energy production ($ES = -\langle U_{sd}U_{sd}\frac{dU}{dr}\rangle$) assuming isotropic velocity fluctuations. The kinetic energy due to the thermal shear effect (amplified by using the square of the standard deviation in lieu of the Reynolds stress) is much smaller, by at least a factor of three, when compared to the kinetic energy due to the thermal buoyant effect. This confirms that the thermal buoyant instability mechanism ($Pr = 0.71$) is responsible for the onset. These results are in agreement with that of linear stability analysis [6] at the same Reynolds number. In the case of assisted flow at $Re = 1000$, Fig. 10 of Su and Chung [6] indicates that for $Pr > 0.3$, the buoyant production term dominates the shear production term and the ratio EB/ES is of the order of three.

Figs. 11–16 have shown that at a low Grashof number, the thermal shear instability created in a buffer region where the velocity profiles include a point of inflexion, disturbs the flow but does not propagate throughout the tube cross section, and damps out because of viscous dissipation. However, by increasing the Grashof number, thermal buoyant fluctuations (due to buoyant turbulence production) increase whereas the thermal shear fluctuations do not change. Temperature fluctuations diffuse and perturb the region for which the viscous dissipation is less important (the buffer and centreline regions). With additional increases of the Grashof number, temperature fluctuations develop throughout the tube

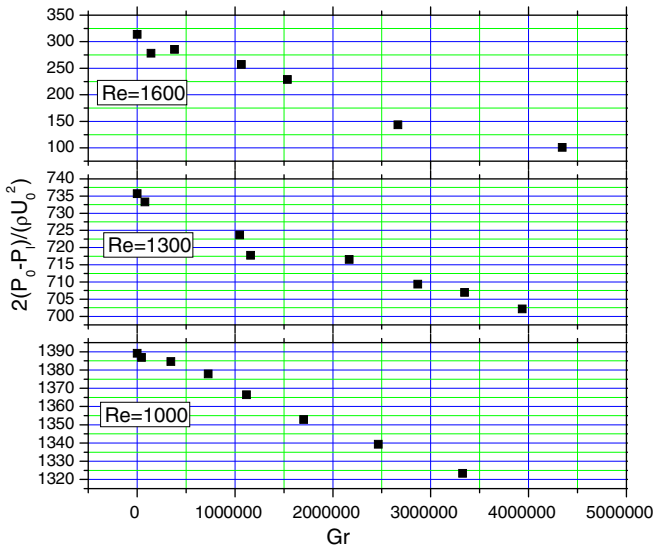

Fig. 19. Non-dimensional inlet and outlet pressure difference.

cross section with a significant frequency (thermal buoyant instability); the viscous dissipation is then augmented while the thermal shear turbulent production is fairly negligible.

Fig. 18 shows the comparison of the temperature spectra at two different axial positions ($Z/D = 6.81$ and $Z/D = 45$) for the case of $Gr = 5.19 \times 10^6$ and $Re = 1609$. The absence of the peak at $Z/D = 6.81$ leads to the conclusion that the periodic phenomenon does not origin from upstream and then cannot be associated to any entrance effects. Two scenarios could be considered for its occurrence: (1) a cell or a wave at a frequency of 0.45 Hz onsets downstream of the location $Z/D = 6.81$ and develops inside tube, (2) an inflow of air that occurs at the tube outlet from the atmosphere and triggers a flow reversal in the tube. The first behavior is also predicted with our numerical calculations [8] for which a laminar flow regime at the tube entrance changes to a turbulent regime downstream.

Fig. 19 shows a static pressure at the tube outlet lower than that at the inlet in the case of the *Re*–*Gr* combinations tested; these measurements allow discarding the second scenario. However since the difference between these two static pressures decreases as the Grashof number increases, future tests with a larger heating power could add the effect of an inflow from the outlet.

4. Conclusion

The instability of the flow in a vertical tube under buoyancy assisted mixed convection has been studied experimentally. The main observations are:

- Using the mean temperature measured at the center of the tube, a "point of deviation" has been detected for flows with $Gr/Re > 1500$.
- A FFT analysis of the temperature signals indicated the presence of a periodic thermal instability with a 0.45 Hz frequency in the range $Gr/Re > 1500$ and its absence in the range $Gr/Re < 1500$.
- This periodic phenomenon cannot be associated to any entrance effects.
- The comparison of three sets of data indicates that the fluctuations are first generated in the buffer region (where a point of inflexion appears in the velocity profile) and then propagate to the centreline region to cause a wavy structure with a significant frequency (0.45 Hz); this wavy structure finally diffuses towards the wall region and covers the entire region with the same dominating frequency (≅0.45 Hz).
- Using the terms of the turbulent kinetic energy equation, the thermal buoyant turbulent production is shown much higher than thermal shear turbulent production.
- The onset of transition at the low Reynolds numbers has been detected and attributed to the thermal buoyant instability.

Acknowledgements

The authors thank the Natural Science and Engineering Research Council of Canada for its financial support as well as the University of Sistan and Baluchestan.

References

[1] B. Metais, E.R.G. Eckert, Forced, mixed, and free convection regimes, ASME J. Heat Transfer 86 (1964) 295–296.
[2] G.F. Scheel, T.J. Hanratty, Effect of natural convection on stability of flow in a vertical pipe, J. Fluid Mech. 98 (1962) 244–256.
[3] L.S. Yao, Is a fully-developed and non-isothermal flow possible in a vertical pipe?, Int J. Heat. Mass Transfer 30 (1987) 707–716.
[4] L.S. Yao, B.B. Rogers, The linear stability of mixed convection in a vertical annulus, J. Fluid Mech. 201 (1989) 279–298.
[5] Yen-Cho Chen, J.N. Chung, The linear stability of mixed convection in a vertical channel flow, J. Fluid Mech. 325 (1996) 29–51.
[6] Yi-Chung Su, L.N. Chung, Linear stability of mixed-convection flow in a vertical pipe, J. Fluid Mech. 422 (2000) 141–166.
[7] M.A. Bernier, B.R. Baliga, Visualization of upward mixed-convection flows in vertical pipes using a thin semitransparent gold-film heater and dye injection, Int. J. Heat. Fluid Flow 13 (1992) 241–249.
[8] A. Behzadmehr, N. Galanis, A. Laneville, Laminar–turbulent transition for low Reynolds number mixed convection in a uniformly heated vertical tube, Int. J. Numer. Meth. Heat. Fluid Flow 12 (2002) 839–854.
[9] A. Behzadmehr, N. Galanis, A. Laneville, Low Reynolds number mixed convection in vertical tubes with uniform wall heat flux, Int. J. Heat. Mass Transfer 46 (2003) 4823–4833.
[10] A. Behzadmehr, N. Galanis, T.C. Nguyen, Predicted effects of inlet turbulent intensity on mixed convection in vertical tubes with uniform wall heat flux, Int. J. Therm. Sci. 45 (2006) 433–442.
[11] D.S.K. Ting, K.C. Cheng, Relaminarization of developing turbulent flow in a 180° curved square channel: fluctuation measurements, Exp. Heat Transfer 9 (1996) 267–285.
[12] Airflow Development, Pitot static tube, AL 133/986.
[13] M.A. Paradis, Pressure and Velocity Measurements in Subsonic Flow, Monogram, Mechanical Engineering Department, Université Laval, Québec, Canada, 1973.
[14] T.M. Hallman, Combined forced and free laminar heat transfer in vertical tubes with uniform internal heat generation, ASME Trans. (1956) 1831–1841.